Plasmonics (2014) 9:71–78
DOI 10.1007/s11468-013-9599-6

Highly Sensitive Refractive Index Sensing with Surface Plasmon Polariton Waveguides

Yuee Li · Aning Ma · Lili Yang · Xiaoping Zhang

Received: 15 May 2013 / Accepted: 4 July 2013 / Published online: 16 July 2013

Abstract Two prototypical transducer structures are proposed, including a single-waveguide (SW) and Mach–Zehnder interferometer (MZI), implemented with surface plasmon polariton waveguides. Formulas of the output power with structural parameters are deduced respectively. The sensitivities are found to be proportional to S_1 for SW and S_2 for MZI, which are dependent on waveguide parameters. Maximizing S_1 or S_2 maximizes the corresponding sensitivity, leading to optimized waveguide designs and preferred operating wavelengths. Sensitivity parameters S_1 and S_2 are calculated for fundamental modes of V grooves, triangular wedges, and dielectric-loaded surface plasmon polariton waveguides (DLSPPWs), as a function of measured material refractive index n_c (n_c=1.3~1.6, representative refractive index of biochemical matter), at wavelength λ=1.55 μm. Finally, the sensitivity S_2 is analyzed as a function of work wavelength for DLSPPWs with different ridge thickness and specific fluidic SPP waveguide for biochemical sensing is presented. The results offer foundations for application of surface plasmon polariton waveguides in biochemical sensing.

Keywords Mach–Zehnder interferometer · Surface plasmon polariton waveguide · Waveguide sensors

Introduction

Surface plasmon polaritons (SPPs) are light waves that are coupled to free electron oscillations in a metal, which can be laterally confined below the diffraction limit using subwavelength metal structures. SPPs are prospective methods to accomplish miniaturization and high-density integration of optical circuits [1–3]. Therefore, SPP waveguides have attracted great interest in recent years. A variety of structures such as metal stripes [4, 5], V grooves [1, 6, 7] in a metal surface, triangular wedges [8, 9], and dielectric-loaded surface plasmon polariton waveguides (DLSPPWs) [10, 11] have been proposed and investigated for guiding SPPs.

Given that SPPs are tightly bound to the surface of the metal in the above-mentioned structures, biochemical sensors are often suggested as a good direction for potential applications. Indeed, this direction has led to success of conventional surface plasmon resonance (SPR) sensors. Owing to high loss of SPPs, the conventional approach to SPP sensing rests on the excitation installations of the surface plasma wave and is referred to SPR sensors [12]. Reviews describing the performance of various SPR sensors and interrogation schemes have recently been published [13]. But the prism and its Servo System are causing bottlenecks in high integration and miniaturization of SPR sensing systems.

Meanwhile, the application of optical waveguides, including planar waveguides and fiber gratings, is becoming more widespread in biochemical sensing since it offers the possibility of producing compact, monolithic, multisensor devices which may be connected to instrumentation using optical fibers, allowing remote operation [14]. But the sensitivities of conventional waveguide sensors are not satisfying, because the measured materials were always laid in cladding of the optical waveguide [15–17]. SPP waveguides, as a novel subwavelength structure, have both high sensitivity of SPR sensor and simple structure of optical waveguides. Pierre Berini has explored sensitivities of 1-D SPP waveguides theoretically [18]. Zhao Xu designed a Mach–Zehnder interferometer (MZI) structure consisting of doubly corrugated

Y. Li (✉) · A. Ma · L. Yang · X. Zhang
School of Information Science and Engineering,
Lanzhou University, Lanzhou 730000, China
e-mail: liyuee@lzu.edu.cn

X. Zhang
e-mail: zxp@lzu.edu.cn

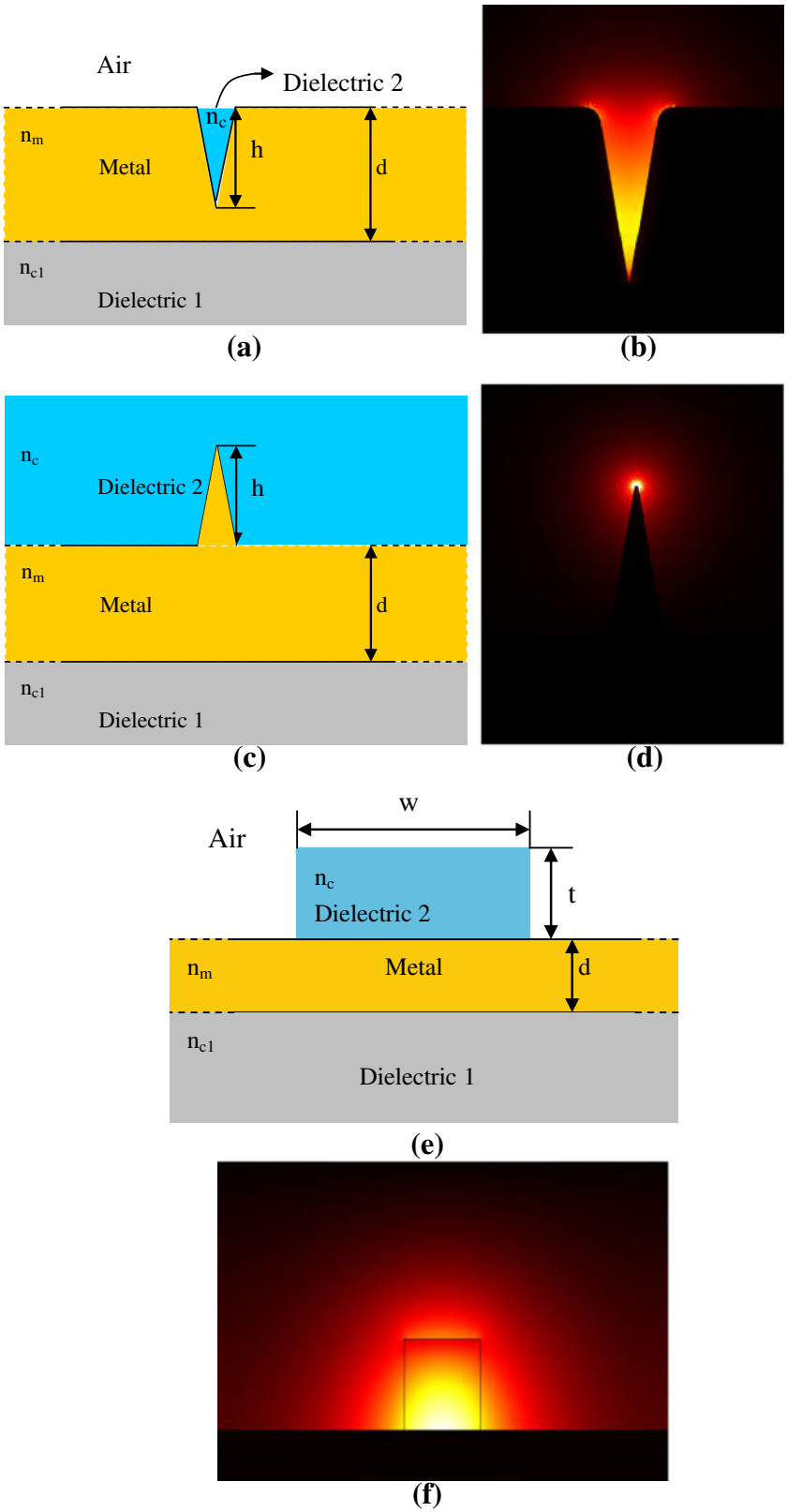

Fig. 1 Sketches of 2-D surface plasmon waveguides and field distribution plots of the magnitude of the electric field |**E**| of the mode of interest (λ_0 (vacuum)=1.55 μm), calculated by COMSOL Multiphysics. The relative permittivity of gold (*yellow*), dielectric 1 (*light gray*), and dielectric 2 (*sky blue*) regions is n_m^2, n_{c1}^2, and n_c^2, respectively. **a**, **b** Subwavelength metal groove of finite depth h=1,200 nm in a metal,the groove angle θ=20°, and gold film thickness d=2 μm. **c**, **d** Triangular metal wedges of finite depth h=1,200 nm in a metal,the groove angle θ=20°, and gold film thickness d=2 μm. **e**, **f** Dielectric-loaded surface plasmon polariton waveguides (ridge dimension w=500 nm, t=600 nm, gold film thickness d=100 nm)

spoofed surface plasmon polariton waveguide [19]. However, the potential of approaches based on 2-D SPP waveguides in biochemical sensing has not been explored. The purpose of this paper is to explore theoretically waveguide refractive index sensors composed of SPP waveguides for biochemical sensing.

Single-waveguide and single-output MZI are adopted as the prototypical transducer structure, and corresponding sensitivity parameters S_1 and S_2 are presented. More particularly, we compared the sensitivities of three popular 2-D SPP waveguides which are suitable for biochemical sensing. From the point of view of waveguide structures, V grooves are more suitable for the fluid to be examined flows through, the apex angle of triangular wedges can be positioned into the fluid, and DLSPPWs are easy to manufacture since they have a similar structure with planar optical waveguides. This is why we consider these 2-D waveguides operating in the fundamental surface mode.

The paper is organized as follows: 2-D SPP waveguides investigated are presented in "Waveguide structures investigated and material parameters" section. Sensitivity parameters S_1 and S_2 are defined in "Theoretical analysis" section. Results as a function of geometry and operating wavelength are comple mented in "Numerical results" section. In "Design of fluidic SPP waveguides for biochemical sensing" section., a specific fluidic SPP waveguide for biochemical sensing is proposed.

Waveguide Structures Investigated and Material Parameters

Figure 1 gives three 2-D SPP waveguides and operating modes of interest. The specific structural parameters used are listed in the caption of Fig. 1. The field distributions of the magnitude of the electric field $|\mathbf{E}|$ of the mode of interest are obtained by COMSOL Multiphysics (RF module: Boundary mode analysis). Considering strong concentration of optical energy in dielectric 2, we are exploring application of surface plasmon polariton waveguides in biochemical sensing. Propagation distance of three 2-D surface plasmon polariton waveguides has been analyzed over a broad wavelength range (Fig. 2a) since it is one of the decisive parameters in waveguide sensors. The relative permittivity of gold varies with work wavelength of surface plasmon polariton waveguides and can be calculated using the Drude–Lorentz Model [20]. At n_c=1.335 (an aqueous solution is typically used as a carrier fluid for the analyte in biochemical sensors), as it is easy to show that propagation distances of V grooves and triangular wedges are much shorter than those of DLSPPWs. A decrease of work wavelength increases the field portion confined in the dielectric 2, and the effective mode index therefore increases (Fig. 2b).

Theoretical Analysis

Single Waveguide

The first prototypical sensor considered is a single waveguide sketched in Fig. 3. It is assumed that the sensor is implemented end to end using a 2-D waveguide sketched in Fig. 1a, c, e. Fluidic channels are also sketched; the fluid to be examined flows through the waveguide. Differences in their bulk index cause changes of the waveguide output power. The length of the sensing region is L, and L_0 (not shown) is the optical path length needed for the input and output access.

The output power of the single waveguide with an attenuation of α (the attenuation cannot be neglected in surface plasmon waveguides) is given by

$$P_{\text{out}} = P_{\text{in}} e^{-2\alpha(L+L_0)} = P_{\text{in}} e^{-2k_0 k_{\text{eff}}(L+L_0)} \quad (1)$$

where P_{out} is measurable in this simple structure, and $\alpha = k_0 k_{\text{eff}}$ is the attenuation constant of plasmon waveguides. The power sensitivity is defined as $\partial P_{\text{out}}/\partial n_c$, which works out to

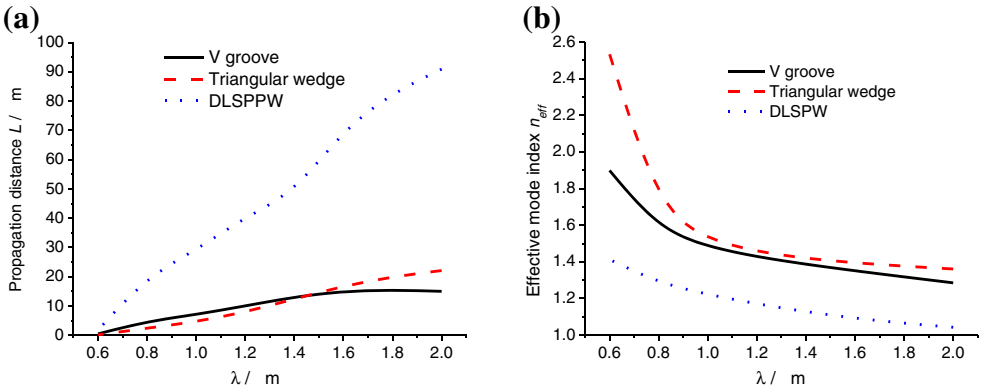

Fig. 2 **a** Propagation distances. **b** Mode effective indexes of V grooves, triangular wedges, and DLSPPWs (n_c=1.335, n_{c1}=1.6)

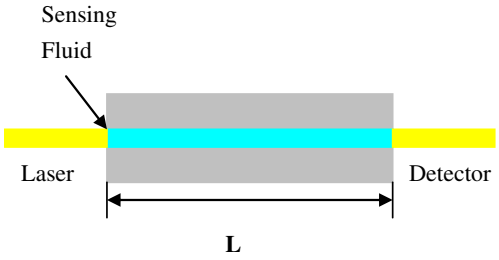

Fig. 3 Sketches of a single waveguide used as a bulk sensor

$$\frac{\partial P_{\text{out}}}{\partial n_c} = \frac{\partial P_{\text{out}}}{\partial k_{\text{eff}}}\frac{\partial k_{\text{eff}}}{\partial n_c}$$

$$= -2P_{\text{in}}k_0(L+L_0)\overbrace{e^{-2k_0k_{\text{eff}}(L+L_0)}}^{U(L)}\frac{\partial k_{\text{eff}}}{\partial n_c} \quad (2)$$

It can be seen that the length of the sensing region L could be selected to maximize $U(L)$. This is achieved by setting $\partial U(L)/\partial L$ to zero and finding the roots:

$$\frac{\partial U(L)}{\partial L} = e^{-2k_0k_{\text{eff}}(L+L_0)}(1-2k_0k_{\text{eff}}(L+L_0)) = 0 \quad (3)$$

which are $L\to\infty$ and $L=1/2k_0k_{\text{eff}}-L_0=1/2\alpha-L_0$. It is easy to confirm that the limit $U(L\to\infty)$ is 0 because the sensitivity vanishes for this length. Inspection of the sign $\partial^2U(L)/\partial L^2$ at $L=1/2k_0k_{\text{eff}}-L_0$ reveals that this solution corresponds to a maximum of $U(L)$; hence, this length is termed as the optimal sensing length. Actually, $1/2k_0k_{\text{eff}}=1/2\alpha$ corresponds to the propagation length of the mode L_e. The maximum value of U is thus

$$U(L=L_e-L_0) = \frac{1}{2k_0k_{\text{eff}}e} \quad (4)$$

Substituting the above into Eq. (2) yields

$$\frac{\partial P_{\text{out}}}{\partial n_c} = \frac{\partial P_{\text{out}}}{\partial k_{\text{eff}}}\frac{\partial k_{\text{eff}}}{\partial n_c} = -P_{\text{in}}\frac{1}{k_{\text{eff}}e}\frac{\partial k_{\text{eff}}}{\partial n_c} \quad (5)$$

which we rewrite as

$$\frac{\partial P_{\text{out}}}{\partial n_c} = \frac{\partial P_{\text{out}}}{\partial k_{\text{eff}}}\frac{\partial k_{\text{eff}}}{\partial n_c} = -P_{\text{in}}\cdot\frac{1}{e}\cdot S_1 \quad (6)$$

defining

$$S_1 = \frac{1}{k_{\text{eff}}}\frac{\partial k_{\text{eff}}}{\partial n_c} \quad (7)$$

S_1 depends on the wavelength-dependent waveguide parameters $\partial k_{\text{eff}}/\partial n_c$ and k_{eff}. From Eq. (6), it is clear that maximizing $|\partial P_{\text{out}}/\partial n_c|$ means maximizing S_1; therefore, the best waveguide design and operating wavelength for surface sensing are those that maximize S_1.

Mach–Zehnder Interferometer

The second prototypical sensor considered is the single-output equal-arm MZI sketched in Fig. 4 [18]. The MZI is implemented end to end using a 2-D waveguide sketched in Fig. 1a, c, e, respectively. Fluidic channels are also sketched overlapping with each arm of the MZI, where one is the sensing arm and the other is the reference arm. L is the length of the sensing arm, and L_0 (not shown) is the optical path length needed for the input and output access, the splitter and combiner. The MZI used as a bulk sensor is shown in Fig. 4. The fluid to be measured flows through the sensing arm, and reference fluid flows through the reference arm. The output power of MZI changes with differences of their bulk refractive index.

Neglecting losses of two Y-branching splitters and assuming that two channels have identical propagation losses, the output power of the MZI implemented with a waveguide having an attenuation of α is given by [18, 21]

$$P_{\text{out}} = P_{\text{in}}e^{-2\alpha(L+L_0)}\frac{1}{2}(1+\cos\phi_D)$$

$$= P_{\text{in}}e^{-2k_0k_{\text{eff}}(L+L_0)}\frac{1}{2}(1+\cos\phi_D) \quad (8)$$

where

$$\phi_D = \frac{2\pi L}{\lambda_0}\left(n_{\text{eff,s}}-n_{\text{eff,r}}\right) \quad (9)$$

It is the difference between the insertion phase of the sensing (s) arm and that of the reference (r). P_{out} is measurable, and $\alpha=k_0k_{\text{eff}}$ is the attenuation constant of surface plasmon waveguides. The phase sensitivity is defined as

$$\frac{\partial P_{\text{out}}}{\partial \phi_D} = -P_{\text{in}}\frac{1}{2}e^{-2\alpha(L_0+L)}\sin\phi_D \quad (10)$$

As is evident from the above, the maximum sensitivity occurs for $\phi_D=\left(n+\frac{1}{2}\right)\pi$ with $n=0, \pm1, \pm2, \pm3,\ldots$ and vanishes for $\phi_D=m\pi$ ($m=0, \pm1, \pm2, \pm3, \ldots$). From Eq. (10), we can observe that the waveguide attenuation

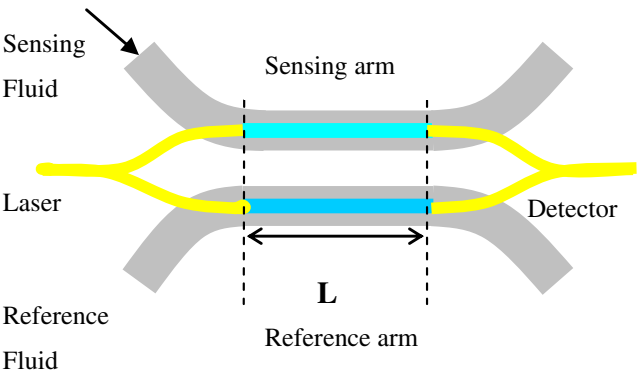

Fig. 4 Sketches of MZIs used as a bulk sensor

leads to a decrease of phase sensitivity compared with a lossless waveguide, in that P_{in} needs to be increased in order to maintain the same phase sensitivity with lossless waveguide MZI.

The MZI bulk sensitivity is defined as $\partial P_{out}/\partial n_c = \partial P_{out}/\partial\phi_D(\partial\phi_D/\partial n_c)$, combining Eq. (9) with Eq. (8) yields

$$\frac{\partial P_{out}}{\partial n_c} = -P_{in}\frac{1}{2}e^{-2\alpha(L_0+L)}\sin\phi_D\frac{2\pi L}{\lambda_0}\frac{\partial n_{eff,s}}{\partial n_c} \tag{11}$$

According to a similar derivation [18], we rewrite Eq. (11) as

$$\frac{\partial P_{out}}{\partial n_c}(L = L_e) = -P_{in}\frac{1}{4}e^{-(1+2\alpha L_0)}(\sin\phi_D)\cdot S_2 \tag{12}$$

defining

$$S_2 = \frac{2\pi}{\lambda_0}\frac{1}{\alpha}\frac{\partial n_{eff,s}}{\partial n_c} = \frac{\partial n_{eff,s}/\partial n_c}{k_{eff}} \tag{13}$$

From Eq. (12), it is clear that maximizing $|\partial P_{out}/\partial n_c|$ means maximizing S_2; therefore, the best waveguide design and operating wavelength for surface sensing are those that maximize S_2 for MZI structure

Numerical Results

Figure 5 gives mode effective indexes and sensing parameters computed for fundamental mode supported by V grooves, triangular wedges, and DLSPPWs as a function of n_c. A

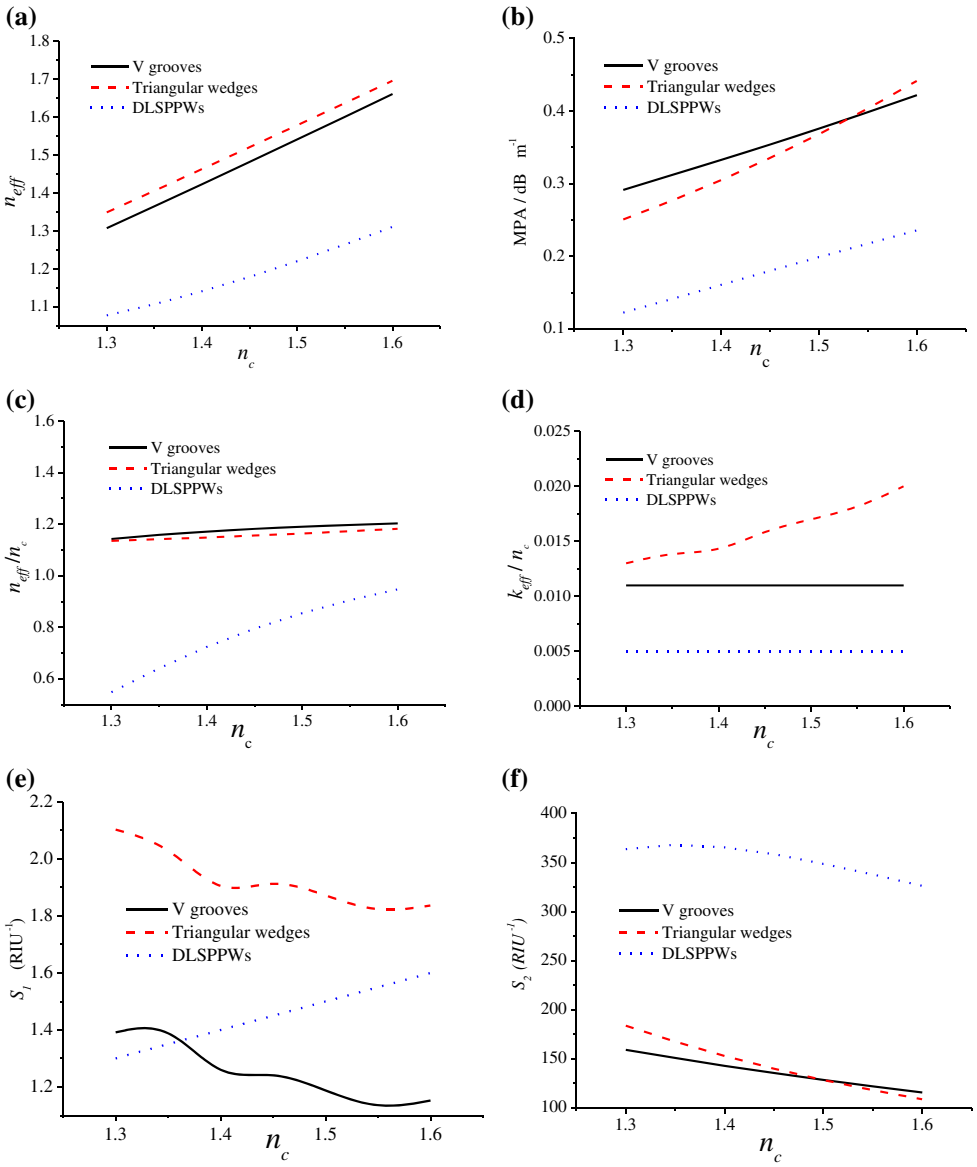

Fig. 5 Mode effective indexes and bulk sensing parameters for V grooves, triangular wedges, and DLSPPWs (sketched in Fig. 1**a**, **c**, **e**). n_{eff} and k_{eff} are computed by COMSOL. MPA is computed using Eq. (8). Other parameters are computed using approximate formulae as follows: **a** $\frac{\partial n_{eff}}{\partial n_c}$ and $\frac{\partial k_{eff}}{\partial n_c}$ with Eqs. (9) and (10), respectively, **b** S_1 with Eq. (7), **c** S_2 with Eq. (13)

representative refractive index range of biological material is adopted n_c=1.3~1.6 [22]. The mode power attenuation (MPA) in decibel above 1 mW is given by

$$\mathrm{MPA} = \alpha 20\log_{10} e \tag{14}$$

n_{eff} and k_{eff} are obtained using COMSOL (software based on FEM). $\partial n_{\mathrm{eff}}/\partial n_c$ and $\partial k_{\mathrm{eff}}/\partial n_c$ are computed directly by central finite-difference formula

$$\frac{\partial n_{\mathrm{eff}}}{\partial n_c} \doteq \frac{n_{\mathrm{eff}}(n_c + h_c) - n_{\mathrm{eff}}(n_c - h_c)}{2h_c} \tag{15}$$

and

$$\frac{\partial k_{\mathrm{eff}}}{\partial n_c} \doteq \frac{k_{\mathrm{eff}}(n_c + h_c) - k_{\mathrm{eff}}(n_c - h_c)}{2h_c} \tag{16}$$

The spacing h_c may be variable or constant. These approximations improve in accuracy when $h_c \to 0$. In the computations, we use $h_c = 10^{-3} \ll n_c$.

As expected, both the mode effective index and MPA increase as n_c increases because the fundamental modes are more tightly confined at large n_c. As shown in Fig. 5b, MPA of the fundamental mode supported by DLSPPW is lower by factors of about 2–3 than that of other two structures. So the propagation distance is larger, which makes for waveguide sensing. The fundamental mode supported by triangular wedges poses larger $\partial k_{\mathrm{eff}}/\partial n_c$, and consequently, the S_1 of triangular wedges is larger than that of the other two structures, as is evident from Fig. 5d, e. As shown in Fig. 5c, $\partial n_{\mathrm{eff}}/\partial n_c$ of the fundamental mode supported by V grooves and triangular wedges is larger on the small side than that of DLSPPW because of better field confinement, whereas S_2 of DLSPPW is larger by factors of about 2–3 because of smaller k_{eff} or MPA. The largest value of S_2 and S_1 can be obtained at $n_c \approx 1.3 \sim 1.35$, which is the infraction index arrange of aqueous solution widely used in biochemical detecting. Indeed, the value of S_2 and S_1 keep stable for a special waveguide over the range of n_c. Comparing Fig. 5e, f, S_2 is larger by factors of about 100–300 than S_1. Comparing the sensitivities of the MZI structure and single waveguide, we need to go back to Eqs. (6) and (12). Minimize L_0 (the optical path length needed for the input and output access) to obtain $\alpha L_0 \ll 1$. Choosing the material ($n_{\mathrm{eff},r}$) of the reference arm reasonably to get $\phi_D = \left(n + \frac{1}{2}\right)\pi$, then $\sin\phi_D = 1$, rewrite Eq. (12) to.

$$\frac{\partial P_{\mathrm{out}}}{\partial n_c}(L = L_e) = -P_{\mathrm{in}}\frac{1}{4e}\cdot S_2 \tag{17}$$

It indicates that the MZI structure has larger sensitivity than the single waveguide when two structures have the same input power though its structure is more complicated for manufacture.

Figure 6 gives bulk sensing parameter S_2 computed for the fundamental mode in the DLSPPWs as a function of ridge thickness and operating wavelength λ. In selecting a minimum value for t, consideration must be given to the flow conditions of the carrier fluid (increasing resistance as t decreases), the thickness needed for the receptor layers, and the size of the target biochemical analyte (many nanometers for large biomolecules). Meanwhile, good confinement of field for DLSPPWs must be ensured, and then the smallest value of t considered is 100 nm.

As expected, S_2 decreases with decreasing t (Fig. 6), because the less electric field is confined in the ridge when t decreases. The response of S_2 changes as t decreases: at t=100 nm, S_2 peaks near the short wavelength side, whereas for large t, S_2 has more flat curves and acquires a maximum value across λ=0.8~1.7μm.

Design of Fluidic SPP Waveguides for Biochemical Sensing

A great majority of biochemical materials measured exist in the form of aqueous solutions. In this section, we design a specific SPP waveguide that is composed of fluidic material (detected materials) and Teflon AF with low refractive index n_t=1.31. Figure 7 give the cross-section structure of SPP waveguide and operating mode of interest. The specific structural parameters used are listed in the caption of Fig. 7. Similar to DLSPPW, most of the optical energy strongly concentrates in fluidic material.

Propagation distance, effective mode indexes, and sensitivity S_2 of fluidic SPP waveguides have been analyzed for different w and t at λ_0=1.55 μm (Fig. 8). Effective mode indexes and propagation distances have a slight increase with increasing fluidic material width w. Propagation distances

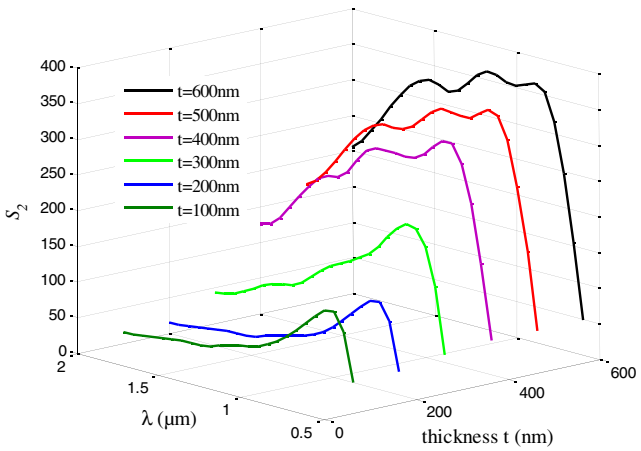

Fig. 6 S_2 for MZI composed of DLSPPWs with different ridge thicknesses across a broad wavelength (n_c=1.335)

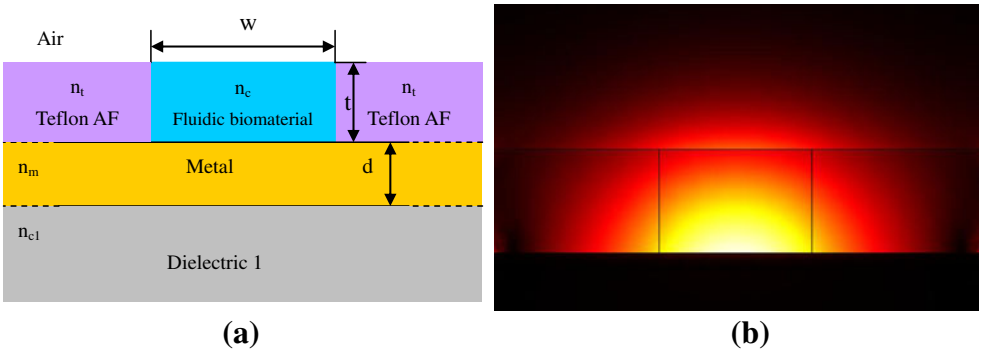

Fig. 7 Sketches of fluidic SPP waveguides and field distributions of the electric field magnitude |**E**| of the mode of interest (λ_0 (vacuum)=1.55 μm), calculated by COMSOL Multiphysics. The relative permittivity of gold (*yellow*), dielectric 1(*light gray*), and dielectric 2 (*sky blue*) regions is n_m^2, $n_{c1}{}^2=1.47^2$, and $n_c^2=1.335^2$, respectively

undergo a clear variation with the increase of t and get a minimum value at around t=400 nm. The sensitivity S_2 increases remarkably with the increases of fluidic material width w, but climbs slightly with the increase of thickness t and reaches saturation at around t=1,000 nm. According to the results, the larger fluidic material size width is preferred. But in the practical application, both the sensitivity and the single-mode propagation should be considered. For example, maximum t is 600 nm for single-mode propagation at w=1,000 nm.

Figure 8 shows that the sensitivity at w=1,000 nm and t=600 nm is still much better than the maximum sensitivity of smaller width (w=300 nm, w=600 nm). If the ridge width is increased more, the maximum t for single-mode propagation will decrease, and the field confinement will be worse [11]. The best width is around w=1,000 nm. In addition, if the measured fluidic materials have a higher refraction index than 1.335, Teflon AF can be substituted for other inexpensive material with low refraction index.

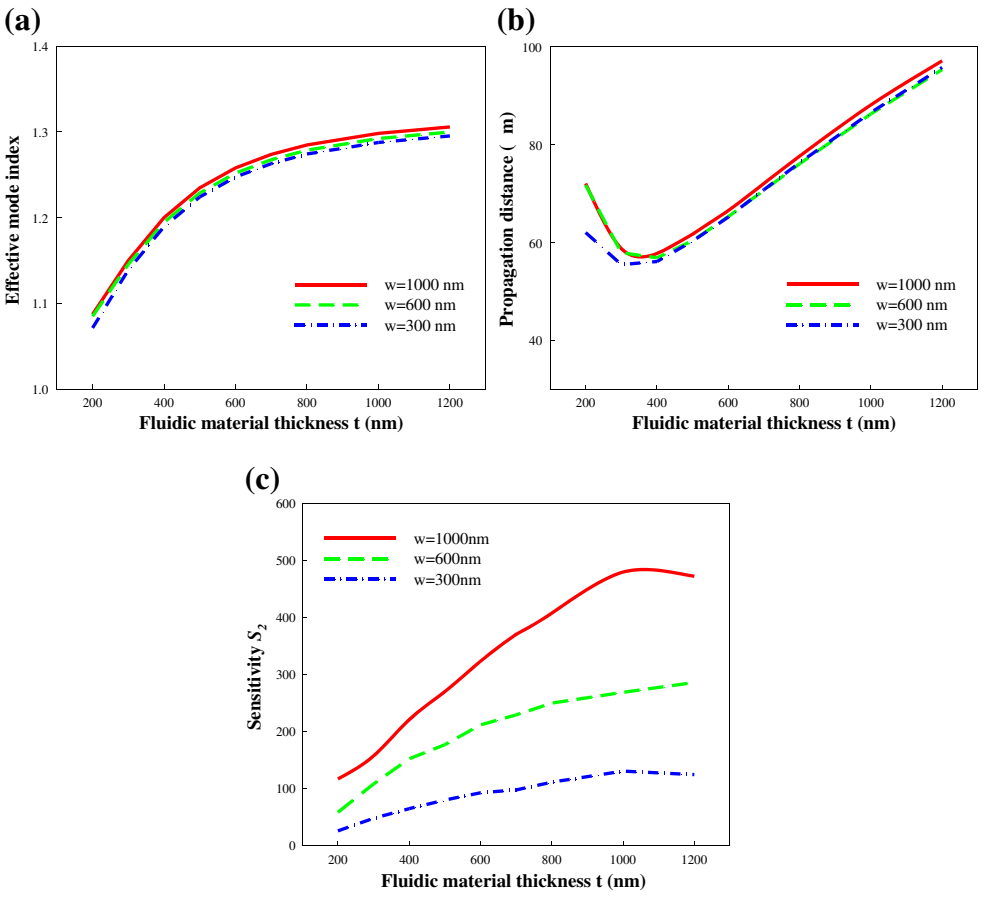

Fig. 8 **a** Propagation distances, **b** effective mode index, and **c** sensitivity S_2 of fluidic SPP waveguides (n_c=1.335, n_{c1}=1.47, λ_0 (vacuum)=1.55 μm)

Conclusion

Investigating the behavior and the sensitivity of SPP waveguides is essential to determine its potential in the different applications. The performance of a single-waveguide and a single-output MZI implemented with SPP waveguides has been presented for infraction index sensing. Two bulk sensitivity parameters S_1 and S_2 are proposed for SW and MZI, respectively. Maximizing S_1 or S_2 maximizes the corresponding sensitivity, leading to preferred waveguide designs and preferred operating wavelengths. Three representative SPP waveguides are assessed and compared theoretically for refractive index sensing, anticipating their use in subwavelength integrated optical waveguide sensors. It was found that the sensitivities in MZI are highly larger than those in SW for all SPP waveguides. On the other hand, S_2 in DLSPPWs exceeds 300 RIU^{-1} and can be three times larger than in the other two waveguides. Furthermore, the bulk sensitivity S_2 is analyzed as a function of operating wavelength λ for various ridge thicknesses. Large bulk sensitivity can be obtained at a broad work wavelength range for sensing. Finally, a specific fluidic SPP waveguide is designed for biochemical sensing at n_c=1.335, and the preferred structure size is discussed. Result analyses and discussions are of great value for exploring high-precision measurement of biochemical material.

Acknowledgments This work was supported by National Natural Science Foundation of China (no. 61210010), the Fundamental Research Funds for the Central Universities (no. lzujbky-2013-42), and China Scholarship Council.

References

1. Bozhevolnyi SI et al (2006) Channel plasmon subwavelength waveguide components including interferometers and ring resonators. Nature 440(7083):508–511
2. Gramotnev DK, Bozhevolnyi SI (2010) Plasmonics beyond the diffraction limit. Nat Photon 4(2):83–91
3. Barnes WL, Dereux A, Ebbesen TW (2003) Surface plasmon subwavelength optics. Nature 424(6950):824–830
4. Degiron A, Berini P, Smith DR (2008) Guiding light with long-range plasmons. Opt Photon News 19(7):28–34
5. Berini P (2000) Plasmon-polariton waves guided by thin lossy metal films of finite width: bound modes of symmetric structures. Phys Rev B 61(15):10484–10503
6. Moreno E et al (2006) Channel plasmon-polaritons: modal shape, dispersion, and losses. Opt Lett 31(23):3447–3449
7. Bozhevolnyi SI (2006) Effective-index modeling of channel plasmon polaritons. Opt Express 14(20):9467–9476
8. Boltasseva A et al (2008) Triangular metal wedges for subwavelength plasmon-polariton guiding at telecomwavelengths. Opt Express 16(8):5252–5260
9. Pile DFP et al (2005) Theoretical and experimental investigation of strongly localized plasmons on triangular metal wedges for subwavelength waveguiding. Appl Phys Lett 87(6):061106
10. Holmgaard T, Gosciniak J, Bozhevolnyi SI (2010) Long-range dielectric-loaded surface plasmon-polariton waveguides. Opt Express 18(22):23009–23015
11. Holmgaard T, Bozhevolnyi SI (2007) Theoretical analysis of dielectric-loaded surface plasmon-polariton waveguides. Phys Rev B 75(24):245405
12. Chien FC, Chen SJ (2004) A sensitivity comparison of optical biosensors based on four different surface plasmon resonance modes. Biosens Bioelectron 20(3):633–642
13. Homola J, Yee SS, Gauglitz G (1999) Surface plasmon resonance sensors: review. Sensors Actuators B: Chem 54(1–2):3–15
14. Zourob M et al (2005) Bacteria detection using disposable optical leaky waveguide sensors. Biosens Bioelectron 21(2):293–302
15. Harris RD, Wilkinson JS (1995) Waveguide surface plasmon resonance sensors. Sensors Actuators B: Chem 29(1–3):261–267
16. Dostálek J et al (2001) Surface plasmon resonance biosensor based on integrated optical waveguide. Sensors Actuators B: Chem 76(1–3):8–12
17. Li XW et al (2011) Integrated plasmonic semi-circular launcher for dielectric-loaded surface plasmon-polariton waveguide. Opt Express 19(7):6549–6556
18. Berini P (2008) Bulk and surface sensitivities of surface plasmon waveguides. New J Phys 1:105010
19. Xu Z, Mazumder P (2012) Bio-sensing by Mach–Zehnder interferometer comprising doubly-corrugated spoofed surface plasmon polariton (DC-SSPP) waveguide. IEEE Trans Terahertz Sci Technol 2(4):460–466
20. Cooper BR, Ehrenreich H, Philipp HR (1965) Optical properties of noble metals. II. Phys Rev 138(2A):A494–A507
21. Born M, Wolf E (1999) Principles of optics: electromagnetic theory of propagation, interference and diffraction of light, 7th (Expanded) Edition. Cambridge University Press, Cambridge. p, 289
22. Arwin H (1986) Optical properties of thin layers of bovine serum albumin, y-globulin, and hemoglobin. Appl Spectrosc 40(3):313–318